Fast Single-Channel Measurements Resolve the Blocking Effect of Cs^+ on the K^+ Channel

Silke Draber and Ulf-Peter Hansen
Institut für Angewandte Physik der Universität Kiel, D-24098 Kiel, Germany

ABSTRACT The Cs^+ block of K^+ channels has often been investigated by methods that allow only indirect estimation of the rate constants of blocking and re-opening. This paper presents single-channel records with high temporal resolution which make the direct observation of the fast transitions between the blocked and the unblocked state possible. The rate constants k_{OGb}, k_{GbO} of Cs^+-dependent blocking and of re-opening are evaluated from the time constants found in the open-time and closed-time histograms. The blocking rate constant k_{OGb} between 1000 and 50000 s^{-1} depends linearly on the Cs^+ concentration and strongly on voltage, increasing by a factor of 1.44 per 10 mV hyperpolarization. The re-opening rate constant $k_{GbO} \approx 30000\ s^{-1}$ is independent of Cs^+ concentration and only slightly voltage-dependent. Formally, the results can be described by a Woodhull-model. The strong voltage dependence with $d > 1$, however, weakens its plausibility. The results are interpreted in terms of a molecular framework emerging from recent results on the structure of voltage-gated channels.

INTRODUCTION

The effect of Cs^+ blocking potassium channels is strongly voltage-dependent. This has been investigated in whole-cell measurements (Hagiwara et al., 1976; Gorman et al., 1982; Cecchi et al., 1987; Tester, 1988) and in single-channel recordings (Yellen, 1984; Demo and Yellen, 1992; Klieber and Gradmann, 1993). Although this effect is unlikely to play any significant physiological role, it has become a model system of blocking effects in general. The marked voltage dependence has been a clue for confirmation or rejection of models about the molecular structure of the channel (Hille and Schwarz, 1978; Tester, 1988). Until now it has not been possible to resolve the fast transitions between the conducting and the blocked state of the channel. Some investigations of the Cs^+ block have been based only on the reduction of the averaged current (Tester, 1988); some have used beta-functions, the distortion of amplitude histograms caused by unresolved short blocking events (Yellen, 1984; Klieber and Gradmann, 1993). All of these studies could not directly see the channel switching between the blocked and the unblocked state. Now, however, a new set-up is available with sampling rates of 100 kHz. Together with a new, more powerful algorithm for jump detection (higher-order Hinkley detector; Schultze and Draber, 1993) and an improved equation for missed-events correction (Draber and Schultze, 1994), these fast transitions can be observed and evaluated directly. Key results of low-noise, high-speed data acquisition are presented in Figs. 2 and 3 below. The Cs^+-induced blocking events that occur at negative voltage (Fig. 3) are not resolved at 5 kHz, but they are resolved at 100 kHz. Fig. 2 shows that the frequent brief closures do not occur at positive membrane voltage.

Received for publication 7 December 1993 and in final form April 4 1994.

Address reprint requests to Silke Draber, Institut für Angewandte Physik, der Universität Kiel, D-24098 Kiel, Germany.

0006-3495/94/07/120/10 $2.00

The new experiments with a temporal resolution of 10 μs were done on excised patches from cytosolic droplets of *Chara corallina*. They confirmed the assumption of Klieber and Gradmann (1993) of fast switching induced by Cs^+. They also resulted in the rate constants of the transitions between open and closed states and in their voltage dependence. The important finding is that the rate constants of the transition between the open state and the Cs^+-induced blocked state have a strong voltage dependence with $d > 1$. This cannot be explained convincingly in terms of the rigid pore of the Woodhull (1973) model. One possibility for explaining extraordinarily strong voltage dependences is the well known assumption of a multi-ion pore (Hille and Schwarz, 1978). We discuss another explanation that takes into account recent results on the molecular structure of the channel.

MATERIALS AND METHODS

Droplets

The experimental set-up and the procedure of obtaining cytoplasmic droplets have been described by Draber et al. (1991). Briefly, cells of *C. corallina*, grown in artificial pond water (0.1 mM KCl, 1.0 mM NaCl, 0.1 mM $CaCl_2$), were cut, and the cytosol was released into a petri dish. In the bathing solution (250 mM KCl, 5 mM $CaCl_2$, 0–25 mM CsCl), the cytosol formed vescicles having a diameter of about 50 μm. The membrane of such vesicles has been shown to consist of tonoplast fragments (Bertl, 1989; Lühring, 1986; Sakano and Tazawa, 1986).

Patch electrodes

Patch electrodes were pulled from borosilicate glass (AR-type, Hilgenberg, Malsberg, Germany) by a L/M-3P-A-puller (List-electronic, Darmstadt, Germany) coated with Sylgard (Dow Corning), fire-polished, and filled with the same solution as in the petri-dish (250 mM KCl, 5 mM $CaCl_2$, 0–25 mM CsCl).

Recording

The investigations were done in the excised configuration (inside-out). The membrane potential V (cytoplasmic side to vacuolar side) was set to different

voltages between −150 and 200 mV by means of a patch-clamp amplifier EPC-7 (List-electronic) and was kept constant for some minutes. After waiting for at least 1 min, the current was recorded for 12–60 s. The signal was low-pass-filtered with a tunable 8-pole switched-capacitor Bessel filter (LTC 1064, Linear Technology) as antialiasing-filter, set to a cutoff frequency (−3 dB) of 25 kHz. The filtered current signal was sampled at 100 kHz and stored on a hard disk for off-line analysis.

Analysis of time series and amplitude histograms

The following four parameters of the recorded current signal are determined by means of an interactive eye-fit procedure. 1) The current I_0 of the baseline (level 0). 2) The single-channel current I_{100kHz}, the distance between the levels. 3) The number, or at least the maximum number, of channels N_{obs} observed to be open simultaneously. 4) The standard deviation σ of background noise.

The eye-fit consists of two stages. First, the time series is displayed (Figs. 3 *A* or 2 *A*) and the levels I_0, $I_0 + I_{100kHz}$, $\cdots$, $I_0 + N_{obs} \cdot I_{100kHz}$ of current are inserted as horizontal lines. It is now possible to change the parameters I_0, I_{100kHz}, N_{obs} interactively until the fitted lines match the current-levels of the record. Second, the amplitude histogram of measured currents (Figs. 3 *C* or 2 *C*) is displayed. The current-levels are shown as vertical lines. The "theoretical amplitude histogram" TAH(I), which is a sum of gaussian distributions

$$\mathrm{TAH}(I) = \sum_{m=0}^{N_{obs}} a_m \frac{1}{\sqrt{2\pi}\sigma} \exp\left(-\frac{1}{2}\left(\frac{I - (I_0 + mI_{100kHz})}{\sigma}\right)^2\right), \quad (1)$$

is superimposed in the same plot. The parameters a_m are not adjusted manually. They are fitted to the measured amplitude histogram by an automatic least-squares optimization. We assume that the background noise is normal distributed (see Eq. 1) with equal standard deviations σ for all levels. This simple assumption does not account for the effects known as beta-distributions (FitzHugh, 1983; Yellen, 1984; Klieber and Gradmann, 1993; Bertl et al., 1993) or open-channel excess noise (Heinemann and Sigworth, 1988). However, this approach yields the value of σ that is required for the improved detection algorithm (Schultze and Draber, 1993) and still allows a reasonable fit of the measured amplitude histogram and a reliable determination of the four parameters I_0, I_{100kHz}, N_{obs}, and σ.

Jump detection and creation of dwell-time histograms

The higher-order Hinkley-detector (H.O.H.D.) (Schultze and Draber, 1993) is applied to the recorded time series (100 kHz). The H.O.H.D. reconstructs the noise-free time series with a time resolution t_{res} that has to be selected according to the signal-to-noise ratio (SNR) and the sampling frequency f_s = 100 kHz to avoid false alarms (Schultze and Draber, 1993; Draber and Schultze, 1994).

$$t_{res} \geq \frac{32/\mathrm{SNR}^2}{f_s}. \quad (2)$$

The detected events can be classified by their levels $m = 0, \cdots, N_{obs}$ and by their type of time course, illustrated by following symbols: open ⊓⊓, closed ⊔⊔, transient ⊓⊔ and ⊔⊓. We lump the transient events with the open- and closed-events in the following way: "Open-events" comprise ⊓⊓, and ⊔⊓, and "closed-events" ⊔⊔, and ⊓⊔. We generate N_{obs} dwelltime histograms of open-events (for level 1 to N_{obs}) and N_{obs} histograms for closed-events (level 0 to $N_{obs} - 1$). In some records with apparently only one active channel in the excised patch, the situation is much easier: there is one histogram for open-events (level 1) and one histogram for closed events (level 0). Below, Fig. 5 shows such a pair of dwell-time histograms.

Determination of rate constants from control measurements without CsCl

The following gating scheme accounts for the three different types of closed events in measurements with 250 mM KCl and 5 mM $CaCl_2$. It is the same model as presented by Draber et al. (1993) and Bertl et al. (1993). C_{long} represents the long-lasting closed state due to deactivation. The states G_f and G_s are "fast" and "slow" gaps, respectively, which are presumably caused by blocking Ca^{2+} ions (Bertl et al., 1993; Laver 1992).

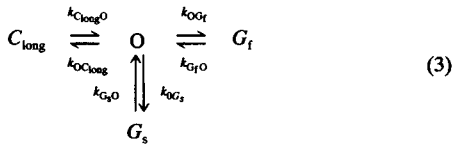

(3)

For each time series of current at a constant voltage, the rate constants are determined. The procedure of obtaining the rate constants starts with exponential fits of the dwell-time histograms. If more than one channel is involved, a special multi-channel joint fit is required (Draber et al., 1993) that makes use of the predominance of short gaps. The slow rate constants are calculated as the inverse of the time constants. The determination of the two fastest rate constants k_{OG_f} and k_{G_fO} accounts for missed events by a new equation developed by Draber and Schultze (1994).

$$\tau_O = \frac{1}{k_{G_bO} - k_{OG_b}}\left[-\frac{2k_{G_bO}}{k_{G_bO} - k_{OG_b}}(1 - \exp(t_{res}(k_{G_bO} - k_{OG_b}))) - t_{res}k_{OG_b} - t_{res}k_{G_bO}\right] + \frac{1}{k_{G_bO} - k_{OG_b}}\left[\frac{k_{G_bO}}{k_{OG_b}}\exp(t_{res}(k_{G_bO} - k_{OG_b})) - 1\right] - t_{res} \quad (4)$$

$$\tau_{G_b} = \frac{1}{k_{OG_b} - k_{G_bO}}\left[-\frac{2k_{OG_b}}{k_{OG_b} - k_{G_bO}}(1 - \exp(t_{res}(k_{OG_b} - k_{G_bO}))) - t_{res}k_{G_bO} - t_{res}k_{OG_b}\right] + \frac{1}{k_{OG_b} - k_{G_bO}}\left[\frac{k_{OG_b}}{k_{G_bO}}\exp(t_{res}(k_{OG_b} - k_{G_bO})) - 1\right] - t_{res} \quad (5)$$

This formula also has special advantages in the case of Cs^+ blockade because both the blocking and the re-opening rate constant are in the same very fast time range.

Plotting the six rate constants obtained from 34 measurements versus voltage shows that the rate constants k_{OG_f}, k_{G_fO}, k_{OG_s}, and k_{G_sO} of gap-kinetics are not voltage-dependent (Fig. 1 *A–D*). They scatter around the following mean values (*horizontal lines* in Fig. 1 *A–D*) with the standard deviation given in percent.

$$k_{OG_f} = 424\ \mathrm{s}^{-1} \pm 29\% \quad (6)$$

$$k_{G_fO} = 31500\ \mathrm{s}^{-1} \pm 32\% \quad (7)$$

$$k_{OG_s} = 222\ \mathrm{s}^{-1} \pm 38\% \quad (8)$$

$$k_{G_sO} = 5150\ \mathrm{s}^{-1} \pm 30\% \quad (9)$$

The scattering of ~±30% reflects the natural fluctuation between different preparations. As can be shown by simulations with appropriate SNR, the accuracy of the analysis (fitting exponentials, etc.) is ~±10% for the rate constants above.

The experiments that are reported here were intended to resolve very fast gating phenomena. Thus, the records are only 12–60 s in length, not long enough for a precise determination of slow rate constants in the 1 s^{-1} range. Although, by this circumstance, the rate constants $k_{OC_{long}}$ and $k_{C_{long}O}$ of deactivation and activation are determined with less accuracy, they are pre-

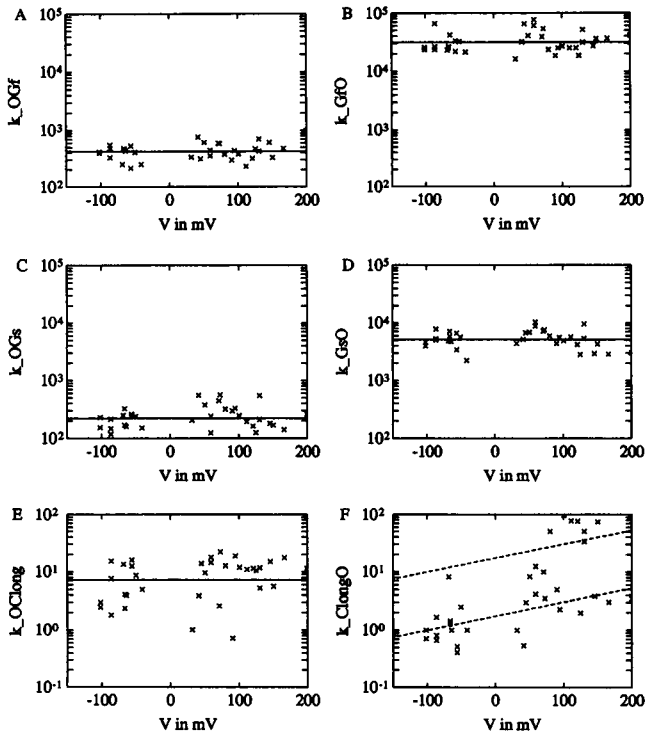

FIGURE 1 Voltage dependence of rate constants obtained without Cs^+. (*A*) k_{OG_f}, (*B*) k_{G_fO}, (*C*) k_{OG_s}, (*D*) k_{G_sO}, (*E*) $k_{OC_{long}}$. These five rate constants are not voltage-dependent; the horizontal lines show the mean values. (*F*) The activation rate constant $k_{C_{long}O}$ is voltage-dependent. The two dashed lines stand for the two conformations (Draber et al., 1993) of the channel.

sented below. The deactivation rate constant plotted in Fig. 1 *E* seems to be independent of voltage:

$$k_{OC_{long}} = 6.5\ s^{-1} \pm 58\%. \quad (10)$$

The activation is voltage-dependent and increases upon depolarization. In addition, the activation is modulated by conformational changes due to cooperativity between channel molecules, as investigated by Draber et al. (1993). The activation rate constant is described by a small voltage dependence, varying between 1 s^{-1} at negative voltages and 4 s^{-1} at positive voltages. This is indicated by the lower dashed line in Fig. 1 *F*. Because of the effect of cooperativity, the channel can change from the usual conformation to the conformation with higher open probability (Draber et al., 1993). Then, the activation rate is increased about 10-fold, shown by the upper dashed line in Fig. 1 *F*. In both conformations, the channel remains an outward rectifier.

During a burst (states *O*, G_f, and G_s), the channels are open for 95% of the time, as calculated from the rate constants in Eqs. 6–9. The gaps G_s and G_f are relatively rare, only for 1 or 4%, respectively, of the time the channels are blocked. This weak block is related to Ca^{2+} (Bertl et al., 1993). Measurements with only KCl in the solution do not show the gaps. Without Ca^{2+}, however, the formation of stable seals is hardly successful and due to a lower seal resistance, the signal-to-noise ratio is worse, which prolongs the time resolution. Therefore, we used 5 mM Ca^{2+} in the solutions. As shown below, the weak Ca^{2+} block is negligible compared with the Cs^+ block at negative voltages.

RESULTS

Cs^+ at positive voltage: no block

A section (100 ms) of a typical record (12 s) of pipette current at positive voltage is shown in Fig. 2 *A*. The gating kinetics of the channel is the same as without Cs^+ in the solution. The results of 11 Cs^+ experiments at positive voltage are in agreement with the values in Eqs. 6–9:

$$k_{OG_f} = 439\ s^{-1} \pm 31\% \quad (11)$$

$$k_{G_fO} = 33200\ s^{-1} \pm 32\% \quad (12)$$

$$k_{OG_s} = 217\ s^{-1} \pm 28\% \quad (13)$$

$$k_{G_sO} = 4950\ s^{-1} \pm 35\%. \quad (14)$$

The slow rate constants $k_{C_{long}O}$ and $k_{OC_{long}}$ have not been calculated here because they are not of interest for investigating the fast Cs^+ block. For positive voltage, we find the same

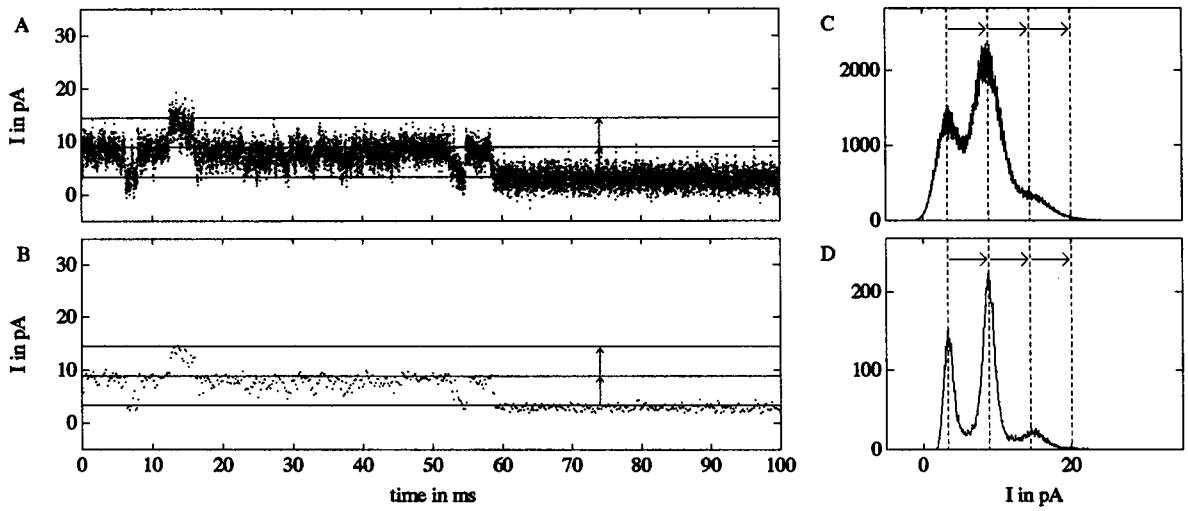

FIGURE 2 Pipette current of a patch with K^+ channels at positive voltage V = 44.8 mV in the presence of 15 mM Cs^+. At positive voltage, the Cs^+ concentration has no influence on the gating kinetics. (*A*) Time series of pipette current sampled at 100 kHz. (*B*) The same section with reduced temporal resolution (sampling rate 5 kHz). (*C*) Amplitude histogram of the whole record (12 s) with high (100 kHz) resolution (see *A*). (*D*) Amplitude histogram with reduced (5 kHz) temporal resolution (see *B*). The single-channel current (*arrows*) of 5.6 pA is the same as in *C*.

gating scheme with or without Cs^+. This supports the hypothesis that the gaps at positive voltage in the presence of Cs^+ (Fig. 2) are caused by Ca^{2+}, not by Cs^+.

By averaging the time series in groups of 20 samples, we reduce the temporal resolution artificially. The sampling rate of the averaged time series is 5 kHz only. The purpose of this averaging becomes obvious in the following section dealing with Cs^+ blockage at negative voltage.

The reduction of the sampling frequency to 5 kHz in Fig. 2 *B* eliminates the short Ca^{2+}-induced gaps (G_f). Averaging over long open-periods (about 1 ms) and brief closed-periods (about 25 μs) has very little effect on the apparent single-channel current. There is no obvious difference between the single-channel current $I_{100kHz} = 5.6$ pA in Fig. 2 *A* and the averaged single-channel current $I_{5kHz} = 5.6$ pA in Fig. 2 *B*. The amplitude histograms (Fig. 2 *C* and *D*) of the whole record (20 s) confirm this result. The peaks corresponding to the levels of current lie at identical positions on the current axis, not affected by averaging. Only the standard deviation σ of noise is reduced.

Cs^+ block at negative voltage: frequent brief gaps

A typical record with the Cs^+-induced gaps at negative voltage is shown in Fig. 3. The original record in Fig. 3 *A* is sampled at 100 kHz. It resolves the very frequent brief gaps.

Again, the time series is averaged in groups of 20. Thus, the sampling rate is reduced to 5 kHz. This procedure results in a record where the fast gaps are no longer visible (Fig. 3 *B*), and the apparent single-channel current I_{5kHz} is an average current over open and closed periods. The construction of this 5-kHz time series is done for two purposes: first, the low-resolution record allows us to compare our results with previous experiments on the Cs^+ effect that have not resolved the brief gaps and, therefore, have only studied the apparent I/V curves with the typical negative slope (Tester, 1988; Klieber and Gradmann, 1993). Second, the fraction $p_{open} = I_{5kHz}/I_{100kHz}$ of the reduced to the true single-channel current gives the open probability of a flickering channel. This quantity is related to the ratio of blocked to unblocked channels $R_B/(1 - R_B) = 1/p_{open} - 1$, which plays an important role in theories on blocking effects (Woodhull, 1973; Tester, 1988).

Averaging in Fig. 3 *B* results in a marked reduction of the apparent single-channel current. The amplitude histograms of the whole 12-s record in Fig. 3, *C* and *D* show that the true single-channel current is $I_{100kHz} = -11.5$ pA and the averaged single-channel current is only $I_{5kHz} = -8.0$ pA. This pronounced reduction allows the calculation of the open probability during a burst; i.e., the fraction of the open-periods as $p_{open} = I_{5kHz}/I_{100kHz} = 0.69$.

I/V Curves

Measurements like those shown in Figs. 2 and 3 were performed at various voltages and at five different concentrations of CsCl: 5, 10, 15, 20, and 25 mM. The resulting single-channel current at full resolution I_{100kHz} and the averaged single-channel current I_{5kHz} are plotted versus the voltage V in Fig. 4. Interestingly, the true single-channel current (full symbols) does not depend on the Cs^+ concentration. The I/V curves are the same as without any Cs^+. They show typical saturation kinetics as predicted by the enzyme-kinetic model (Hansen et al., 1981; Gradmann et al., 1987; Fisahn et al., 1986).

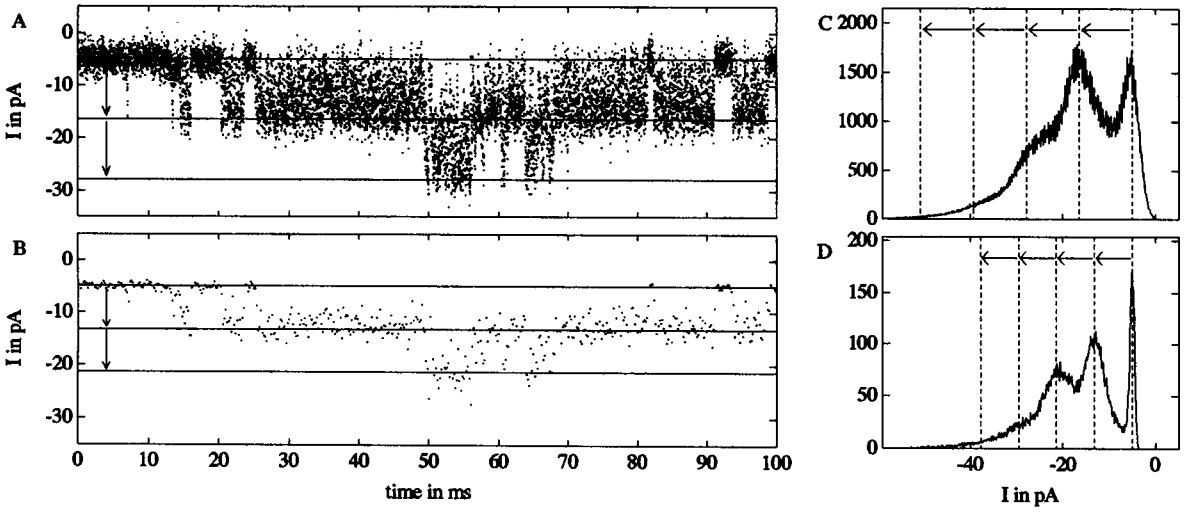

FIGURE 3 Cs^+-induced gating kinetics of the K^+ channel at negative voltage $V = -75.8$. The Cs^+ concentration of 15 mM leads to very frequent brief gaps. (*A*) Section of pipette current sampled at 100 kHz. Plenty short gaps (closures) are visible. (*B*) The same data with reduced temporal resolution (sampling rate 5 kHz). Averaging over closed- and open-periods results in an apparently reduced single-channel current (*vertical arrows at the left*). Brief gaps are no longer visible. (*C*) Amplitude histogram of the whole 12-s experiment with high (100 kHz) resolution (see *A*) single-channel current $I_{100kHz} = -11.5$ pA marked by horizontal arrows. (*D*) Amplitude histogram with artificially reduced temporal resolution (see *B*). The apparent single-channel current $I_{5kHz} = -8.0$ pA (*arrows*) is markedly smaller than in *C*.

The averaged I/V curves (open symbols) show the well known negative slope at negative voltages, which has been observed by several authors before (e.g., Fig. 6 in Klieber and Gradmann, 1993). The new aspect of Fig. 4 is the direct evidence that the single-channel current I_{100kHz} is not reduced by Cs^+, and that the Cs^+ effect on the K^+ channel is a pure gating-phenomenon.

Rate constants of the Cs^+-induced block

The experimental observation of additional Cs^+-induced gaps (Fig. 3) leads to the introduction of an additional state G_b representing the blocked channel. In this state G_b, a Cs^+ ion is bound to the channel protein. Thus, the rate constant k_{OG_b} is a Cs^+-binding rate constant.

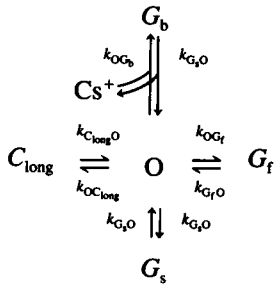

(15)

The closed states C_{long}, G_f, and G_s are already known from the control measurements (compare scheme (3)). Their arrangement has been adopted from Draber et al. (1993) and Bertl et al. (1993).

The determination of the rate constants k_{OG_b} and k_{G_bO} is again based on dwell-time histograms constructed by the H.O.H.D. (Schultze and Draber, 1993). Fig. 5 shows the dwell-time histograms of a measurement with only one channel under observation at a concentration of 10 mM CsCl and a voltage $V = -61$ mV. The time resolution in this case is $t_{res} = 10$ μs. Although the Cs^+ block is quite moderate at this concentration and voltage, the Cs^+-induced gaps already contribute more than 90% of the gaps. This is shown by the following analysis of the dwell-time histogram. The dwell-time histograms are fitted with one open-time constant τ_O = 231 μs and two closed-time constants τ_{G_s} = 284 μs and τ_{G_f} = 23.1 μs. The percentage of fast gaps is 98%. The time

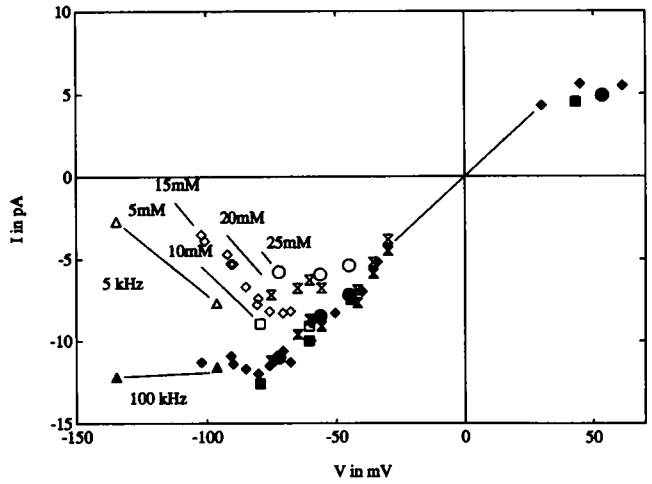

FIGURE 4 Current-voltage curves for different Cs^+ concentrations. (△) 5 mM Cs^+; (□) 10 mM Cs^+; (◇) 15 mM Cs^+; (⧖) 20 mM Cs^+; (○) 25 mM Cs^+. At 100-kHz resolution (*filled symbols*), the open-channel current does not depend on the Cs^+ concentration. Averaging over the Cs^+-induced gaps at 5-kHz resolution (*open symbols*), however, gives the well known negative slope. The Cs^+ block depends on Cs^+ concentration and membrane voltage V.

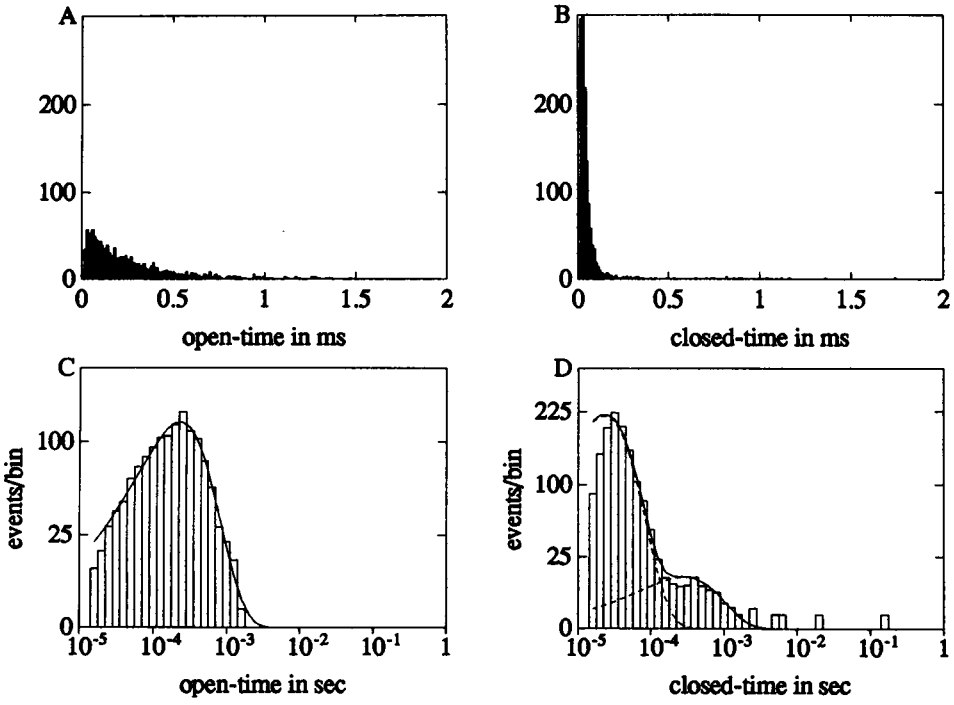

FIGURE 5 Dwell-time histograms of a measurement with only one active channel at $V = -61$ mV and 10 mM Cs^+. (*A*) The open-time histogram can be fitted by a single exponential with τ_O = 231 μs. (*B*) The closed-time distribution can be fitted with a dominant short time-constant of τ_{G_b} = 23.1 μs. The second component of longer closed-events G_s about 300 μs is faintly visible. (*C*) The open-time histogram binned on a logarithmic time scale and with a square-root axis for the events per bin. In this kind of plot, which was suggested by Sigworth and Sine (1987), the exponential distribution of A transforms to one broad peak. The solid line is a fit with τ_O = 231 μs. (*D*) The closed-time histogram displayed on a logarithmic axis shows that there is one dominant short time constant τ_{G_b} = 23.1 μs and at least one slower exponential τ_{G_s} = 284 μs. The two events on the right are due to the slow activation time constant ($\tau_{C_{long}}$).

constant $\tau_{C_{long}}$ is not determined by this fit because during the short measurement there were only few long closed events. Calculation of the rate constants yields $k_{OG_f} = 7160\ s^{-1}$. $k_{G_fO} = 51305\ s^{-1}$, $k_{OG_s} = 146\ s^{-1}$, $k_{G_sO} = 3521\ s^{-1}$. The slow gaps are obviously not affected by Cs^+. The frequency of fast gaps, however, is drastically increased (about 7000 gaps/s during a burst) compared to the Cs^+-free measurements (only 500 gaps/s). Thus, the majority of fast gaps, more than 90%, can be assigned to the Cs^+ block. Therefore, we now call the fast time constant of the closed-time histogram $\tau_{G_b} = 23.1\ \mu s$.

In the following, we determine the rate constants k_{OG_b} and k_{G_bO} describing the Cs^+ block. The transition into the Cs^+-blocked state G_b and back to the open conformation O dominate the dwell-time histograms by far (Fig. 5). As a consequence, all other transitions can be neglected because they have no significant influence on the resulting rate constants k_{OG_b} and k_{G_bO}.

We take the time constants τ_O and τ_{G_b} from the dwell-time histograms and calculate the rate constants of blocking k_{OG_b} and unblocking k_{G_bO}. This procedure has to account for the final temporal resolution t_{res} of the detector (Colquhoun and Sigworth, 1983; Blatz and Magleby, 1986). In the case of the Cs^+-blocked K^+ channel, we are faced with the situation that both the gaps and the open-events between the gaps are short compared to the time resolution. In this situation, the dwell-time omission theories based on the assumption of a fixed dead time of the detector (Colquhoun and Sigworth, 1983; Roux and Sauvé, 1985; Blatz and Magleby, 1986; Yeo et al., 1988; Milne et al., 1989; Crouzy and Sigworth, 1990; Hawkes, Jalali and Colquhoun, 1990; Ball et al., 1993) give incorrect results (Magleby and Weiss, 1990). By means of an improved correction algorithm for missed events (Eqs. 4 and 5), which is based on a realistic model of a detector (Draber and Schultze, 1994), we have determined the rate constants k_{OG_b} and k_{G_bO} from the experiments at 5, 10, 15, and 20 mM Cs^+.

The fast rate constants of the Cs^+ block, k_{OG_b} and k_{G_bO}, were not extracted from the measurements at 25 mM Cs^+ because they show a strong Cs^+ effect already at small negative voltage. The related small single-channel current (bad signal-to-noise ratio) prevents a reliable estimation of these parameters.

Blocking rate constants are normally assumed to depend linearly on the concentration of the blocking agent. We check this by dividing the rate constants k_{OG_b} by the concentration $[Cs^+]$ and by plotting these normalized blocking rate constants $k_{OG_b}/[Cs^+]$ versus the voltage in Fig. 6. On the semilogarithmic plot, the symbols for the four concentrations lie on one descending line. Because $k_{OG_b}/[Cs^+]$ is obviously independent of the Cs^+ concentration, the concentration dependence of k_{OG_b} is proven to be linear, clearly not quadratic (Klieber and Gradmann, 1993).

The data in Fig. 6 is fitted by an exponential voltage-dependence

$$\frac{k_{OG_b}}{[Cs^+]} \sim \exp\left(-d_{OG_b}\frac{eV}{kT}\right), \qquad (16)$$

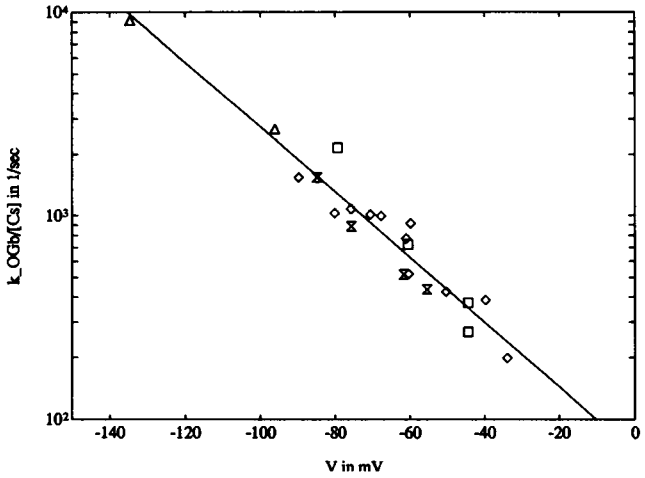

FIGURE 6 The normalized blocking rate constant $k_{OGb}/[Cs^+]$ versus voltage V at different Cs^+ concentrations ($[Cs^+]$ in mM). (△) 5 mM Cs^+; (□) 10 mM Cs^+; (◇) 15 mM Cs^+; (⧖) 20 mM Cs^+. The straight line in the semilogarithmic plot shows a fit with $k_{OG_b}/[Cs^+] = 68.6\ s^{-1}\exp(-0.92eV/kT)$. The concentration dependence of k_{OG_b} itself is linear. The strong voltage dependence is exponential.

with $[Cs^+]$ being the Cs^+ concentration in mM, the membrane voltage V in mV, the elementary charge $e = 1.60\cdot10^{-19}$ As, the Boltzmann constant $k = 1.38\cdot10^{-23}$ J/K, the absolute temperature $T \approx 290$ K, and $kT/e = 25$ mV.

The voltage dependence d_{OG_b} and a confidence interval are determined by a linear regression in the semilogarithmic plot: $d_{OG_b} = -0.92 \pm 0.06$ (standard deviation). The result for the rate constant is

$$k_{OG_b} = 68.6\ s^{-1}[Cs^+]\exp\left(-0.92\frac{eV}{kT}\right). \qquad (17)$$

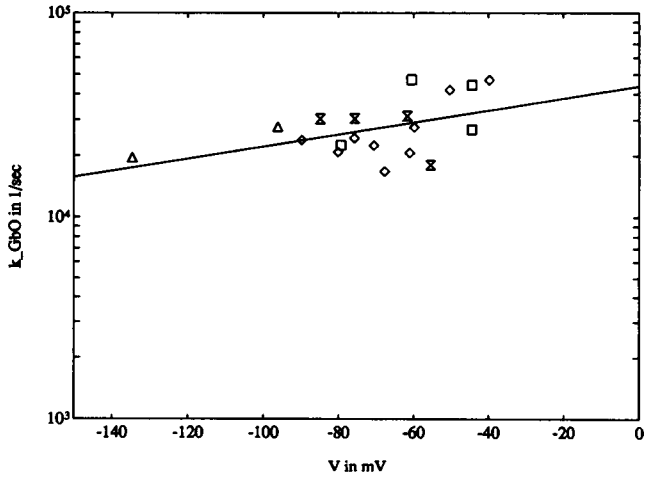

FIGURE 7 The rate constant k_{G_bO} of re-opening versus voltage V at different Cs^+ concentrations. (△) 5 mM Cs^+; (□) 10 mM Cs^+; (◇) 15 mM Cs^+; (⧖) 20 mM Cs^+. There is no obvious dependence on the Cs^+ concentration. The slight voltage dependence is $k_{G_bO} = 43900\ s^{-1}\exp(0.17eV/kT)$.

The deviations between the experimental results and the curve according to Eq. 17 are within the accuracy of about 30%, which is typical for rate constants (see Eqs.6–9).

In Fig. 7, the opening rate constant k_{G_bO} is plotted versus voltage. The data from different Cs^+ concentrations do not suggest any concentration dependence, and the voltage-dependence is weak:

$$k_{G_bO} = 43900\ s^{-1} \exp\left(0.17 \frac{eV}{kT}\right). \quad (18)$$

Data from 19 measurements resulted in the voltage dependence $d_{G_bO} = 0.17 \pm 0.08$ (standard deviation).

Open probability

In the previous sections we have used two independent approaches to evaluate the Cs^+ effect. The first approach is the reduction of the apparent single-channel current in Fig. 4. The second approach is the direct determination of the rate constants k_{OG_b} and k_{G_bO} from the 100 kHz records (Figs. 6 and 7). It is essential to prove that both approaches are consistent. The symbols △, □, ◇, ⧖, and ○ in Fig. 8 show the open probability that can be obtained from the I/V curves in Fig. 4 as $p_{open} = I_{5kHz}/I_{100kHz}$. The solid lines show the open probability calculated from the directly determined rate constants according to Eqs. 17 and 18:

$$p_{open} = \frac{k_{G_b0}}{k_{G_b0} + k_{OG_b}} = \frac{1}{1 + k_{OG_b}/k_{G_b0}} = \frac{1}{1 + (68.6/43900)[Cs^+]\exp(-1.09eV/kT)}. \quad (19)$$

Fig. 8 shows a good agreement of the results obtained by either method.

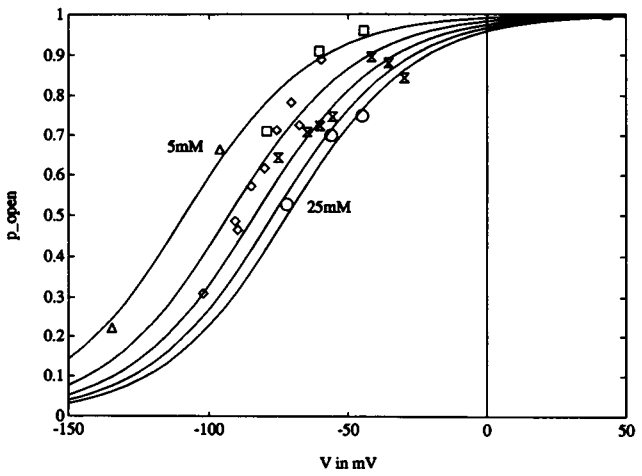

FIGURE 8 Open probability versus voltage for different Cs^+ concentrations. (△) 5 mM Cs^+; (□) 10 mM Cs^+; (◇) 15 mM Cs^+; (⧖) 20 mM Cs^+; (○) 25 mM Cs^+. The symbols are experimental results, obtained from I/V curves (Fig. 4) as the quotient of the averaged current at 5 kHz and the true single-channel current at 100 kHz: $p_{open} = I_{5kHz}/I_{100kHz}$. The lines are calculated by means of Eq. 19 with the data from the fits in Figs. 6 and 7.

DISCUSSION

The Woodhull-model

A well known model of voltage-dependent blockade was developed by Woodhull (1973). The blocking ion has to penetrate into the pore, and reaches its binding site by traveling through a part of the transmembrane electric field. This part is given by the constant d ($0 < d < 1$). Assuming that the channel is a rigid pore whose conformation is altered neither by permeating or blocking ions nor by the electric field, and making use of the concept of energy barriers and energy minima (as applied by Hille and Schwarz, 1978), leads to

$$k_{OG_b} \sim \exp\left(-d_{OG_b} \frac{eV}{kT}\right) \quad (20)$$

$$k_{G_bO} \sim \exp\left(d_{G_bO} \frac{eV}{kT}\right), \quad (21)$$

with d_{OG_b} and d_{G_bO} giving the location of the energy barrier between pore mouth and binding site. The sum $d = d_{OG_b} + d_{G_bO}$ is the whole way the ion has to travel through the pore.

$$\frac{k_{OG_b}}{k_{G_bO}} \sim \exp\left(-d \frac{eV}{kT}\right) \quad \text{with} \quad 0 < d < 1 \quad (22)$$

Concerning the exponential type of the voltage dependence, our results with $d_{OG_b} = -0.92 \pm 0.06$, $d_{G_bO} = 0.17 \pm 0.08$, $d = 1.09 \pm 0.14$ obtained from Figs. 6 and 7 are in agreement with the Woodhull model above. The strong voltage dependence, however, with $d_{OG_b} \approx 1$ cannot be explained satisfactorily by the single-ion Woodhull model. The energy barrier between the external solution and the binding site would be close to the internal mouth of the channel. The blocking site would be located near the internal surface $d \approx 1$. This is hard to imagine taking into account that Cs^+ ions do not permeate the channel.

In the following, we discuss two different models which extend the basic approach of Woodhull (1973) to explain the strong voltage dependence of the Cs^+ block.

More Ions—more voltage dependence

A traditional explanation for strong voltage dependences is the model developed by Hille and Schwarz (1978), who combined the ideas of Woodhull (1973) with the concept of multi-ion pores (Hodgkin and Keynes, 1955). It is assumed that more than one ion can occupy the channel simultaneously (Armstrong and Taylor, 1980). Still, the channel is believed to be a static pore.

If the blocking ion has bound to the blocking site, it is possible that other ions enter the pore. This hinders the spontaneous separation of the blocking ion from its binding site and leads to a prolongation of the blocking time. Thus, the Cs^+-blocked state of the K^+ channel could be characterized by a Cs^+ ion at the blocking site and another ion at a second site as sketched in Fig. 9. Such a model has been used for the Cs^+-blocked K^+ channel by Demo and Yellen (1992). If the fractions of voltage that the ions have passed coming from the external solution are $d_1 = 0.81$ for the blocking Cs^+

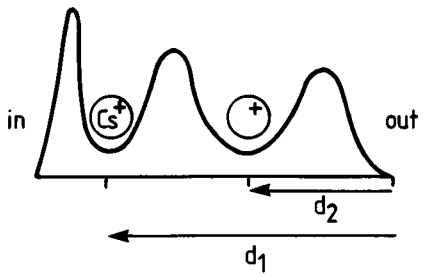

FIGURE 9 Blocked state of a multi-ion pore. The blocking Cs^+ ion has crossed the distance d_1 before reaching the blocking site. The second ion (Cs^+ or K^+) in the pore occupies a site with a voltage dependence of d_2.

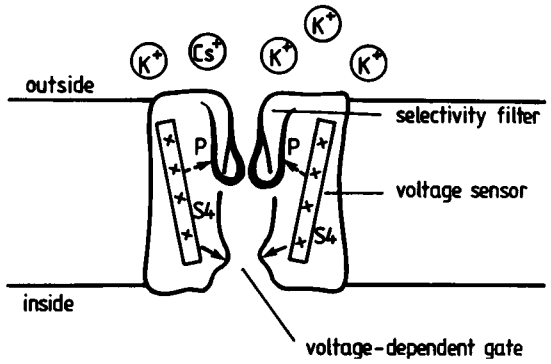

FIGURE 10 Relevant structures for the Cs^+ block: The voltage sensor S4 and the selectivity filter P (pore). This cross section shows only two of the four subunits, which are arranged symmetrically around the central ion pathway. The arrows indicate our hypothesis that the voltage sensor, when responding to membrane voltage, causes conformational changes near the voltage-controlled gate (Durell and Guy, 1992) and in the selectivity filter P (according to the results in this paper). The structural change of the selectivity filter modifies the rate constant k_{OC_s} of Cs^+ blocking the channel.

ion and $d_2 = 0.38$ for the second ion (Demo and Yellen, 1992), the total voltage dependence of this blocked state is $d = d_1 + d_2 = 1.19$. The strong voltage dependence observed in our experiments could be explained by such a model.

This kind of multi-ion explanation, however, requires a deep binding site for the blocking ion. With $d_1 \approx 0.2$, for instance, even the multi-ion explanation would not yield the strong voltage dependence. Another argument against a pure explanation via a multi-ion pore is supplied by Draber et al. (1991), who investigated the anomalous mole-fraction effect of Tl^+ in the K^+ channel. It could be shown by simulating I/V curves that the assumption of a multi-ion pore is not sufficient to explain the Tl^+ effect. Instead, a modulation of the gating scheme had to be assumed that was faster than the time resolution of the experimental setup. This does not rule out that the K^+ channel could in fact be a multi-ion pore but makes obvious that the gating also has to be taken into account.

Flexible channel protein—more voltage dependence

We postulate an alternative explanation for the strong voltage dependence that is not based on a multi-ion assumption. Our hypothesis of a flexible channel protein that responds to membrane voltage by conformational changes is supported by results on the molecular structure of K^+ channels. The important molecular features of K^+ channels are shown in Fig. 10. They have emerged from genetic techniques like point mutations of the channel protein (MacKinnon and Miller, 1989; MacKinnon, 1991; Goldstein and Miller, 1992; Kirsch et al., 1992; De Biasi et al., 1993) or point mutations of the specific blocker charybdotoxin CTX (Park and Miller, 1992; Goldstein and Miller, 1993). The results obtained by these methods together with earlier hydrophobicity plots (e.g., Tanabe et al., 1987) have led to the general insight that all voltage-gated ion channels (mainly the common Na^+, K^+ or Ca^{2+} channels) are members of a quite homologous family of proteins (MacKinnon, 1991; Miller, 1991; Jan and Jan, 1992). Although the K^+ channel in *Chara* has not been analyzed so far, the molecular and functional concepts that have been found in animal channels can also be applied to plant channels because the amino acids in the functionally important parts are highly conserved among different types of K^+ channels (Durell and Guy, 1992; Kirsch et al., 1992). A study emphasizing the analogy between plant and animal K^+ channels was performed by Anderson et al. (1992), who have expressed a plant channel in *Saccharomyces cerevisiae* that has a sequence very similar to the well known *Shaker* K^+ channel from *Drosophila*. The K^+ channels, including the Ca^{2+}-activated high conductance type, studied in this paper, are tetramers consisting of four equal subunits of about 500 amino acids each (MacKinnon, 1991). The subunits have the N-terminal end on the cytoplasmic side, six membrane-spanning α-helices S1, S2, S3, S4, S5, S6 and the C-terminus again on the cytoplasmic side (MacKinnon and Miller, 1989; Miller, 1991; Jan and Jan, 1992).

The main functional parts, shown in Fig. 10, are the selectivity filter and the voltage sensor acting on a voltage-controlled gate.

The structural changes in response to membrane voltage are related to the voltage sensor in the S4-helix (Miller, 1991; Jan and Jan, 1992). The channel feels the membrane voltage by the electric forces on the positive charges of the S4 helices and reacts by changing its conformation in response to voltage. A well known consequence of positive voltage acting on the voltage sensor is the opening of outward rectifying channels. Durell and Guy (1992) have combined molecular and experimental information and have computed a molecular structure for the channel protein by modeling the electrostatic forces between the parts of the molecule. According to their calculations, positive voltage makes the S4 helices move to the external side and, as a consequence, small α-helices called S45 are drawn away from the internal mouth of the channel, i.e., the voltage-controlled gate opens. The involvement of such a voltage sensor has also to be assumed for the K^+ channel in *Chara* because this channel is an outward rectifier. In addition, a similar structure for plant K^+ channels is found for example by Anderson et al. (1992).

Because Cs^+ ions are not transported by the K^+ channel, the Cs^+ block is presumably caused by Cs^+ ions trapped in the selectivity filter of the channel protein. Point mutations (e.g., Kirsch et al., 1992) have shown that the selectivity filter is formed by the P-loop between the helices S5 and S6 (outside, vacuolar side, earlier called H5 loop). The four hydrophilic P-loops, one from each subunit, form the channel mouth on the outer side and are believed to extend some way into the pore like hairpins forming the lining of the pore.

Recent results concerning the location of the blocking Cs^+ ion in the pore are provided by De Biasi et al. (1993). Point mutations have shown that the amino acid at position 369 (9_P in the nomenclature used by Durell and Guy (1992)) is very important for Cs^+ selectivity. Therefore, we assume that the site for the blocking Cs^+ ion is relatively near position 369. To obtain values for a working model, the geometrical distance of the blocking site from the external surface can be assumed to be about 20% according to the structure favored by Durell and Guy (1992). This estimation is in accordance with the results of De Biasi et al. (1993), who found that blockage by Zn^{2+} ions binding to the mutated amino acid at position 369 does not show a significant voltage dependence.

If the findings of De Biasi et al. (1993) are interpreted in terms of the Woodhull model (Eq. 22), a weak voltage dependence of the Cs^+ block is expected with d about 0.2. Our re-opening rate constant has a weak voltage dependence $d_{G_bO} = 0.17 \pm 0.08$, which is well in accordance therewith. But the strong voltage dependence $d_{OG_b} = 0.92 \pm 0.06$ of the blocking rate constant k_{OG_b} is much stronger than could be expected.

This discrepancy leads us to an interpretation that postulates that the voltage dependence due to the model of Woodhull (1973) is supplemented by a term $S(V)$ representing a voltage-dependent structural change, i.e., an allosteric effect of the voltage on the Cs^+ block.

$$k_{OG_b} = 68.6\ s^{-1}\,[Cs^+]\exp\left(-d_w \frac{eV}{kT}\right) \cdot S(V) \qquad (23)$$

with

$$S(V) = \exp\left(-d_s \frac{eV}{kT}\right) \qquad (24)$$

The experimentally obtained d_{OG_b} is now interpreted as the sum of $d_w \approx 0.1$ resulting from the Woodhull model and $d_s \approx 0.8$ resulting from the structural changes.

To give a molecular interpretation of the factor $S(V)$ we postulate that the voltage-dependent shift of the S4-helix (voltage sensor) causes structural changes in the selectivity filter (P) (Fig. 10). This change modulates the access of Cs^+ to its binding site.

CONCLUSION

It is still a matter of controverse discussion if the pore is a "long" or a "short beta-barrel" (Durell and Guy, 1992) and if the Cs^+-binding site is deep inside the pore (Kirsch et al., 1992) or at the surface (De Biasi et al., 1993).

The multi-ion models of Hille and Schwarz (1978) or Demo and Yellen (1992) are more in line with a long beta-barrel and a deep blocking site (Fig. 9). We give an explanation for the strong voltage dependence of the Cs^+ block that supports a short beta-barrel (Durell and Guy, 1992) and a Cs^+ binding site near the external surface. The assumption of a multi-ion pore is not required in our model. If the blocking Cs^+ ion sticks in the selectivity filter near the external mouth of the pore, it seems relatively unlikely that a second ion can simultaneously enter the pore from the external solution. The multi-ion pore model is not applicable. In addition, the assumption of a multi-ion pore with a binding site for the blocking ion at a depth of about 20% leads to a voltage dependence of at most $d \approx 0.3$. This is a too weak voltage dependence for our results of the Cs^+ block.

All of these arguments, especially those based on the results of De Biasi et al. (1993), have led us to the conclusion that conformational changes are an important mechanism for the influence of voltage on the Cs^+ block.

We thank Dr. Roland Schultze for the cooperation in the development of methods for data analysis and for many helpful discussions. Dipl.-Phys. A. Albertsen has constructed the equipment for data acquisition at 100 kHz. We also thank Mrs. E. Götting for drawing Figs. 9 and 10. The investigations were supported by the Deutsche Forschungsgemeinschaft (Ha 712/7-5).

REFERENCES

Anderson, J. A., S. S. Huprikar, L. V. Kochian, W. J. Lucas, and R. F. Gaber. 1992. Functional expression of a probable *Arabidopsis thaliana* potassium channel in *Saccharomyces cerevisiae*. *Proc. Natl. Acad. Sci. USA.* 89:3736–3740.

Armstrong, C. M., and S. R. Taylor. 1980. Interaction of barium ions with potassium channels in squid giant axons. *Biophys. J.* 30:473–488.

Ball, F. G., G. F. Yeo, R. K. Milne, R. O. Edeson, B. W. Madsen, and M. S. P. Sansom. 1993. Single ion channel models incorporating aggregation and time interval omission. *Biophys. J.* 64:357–374.

Bertl, A. 1989. Current-voltage relationships of a sodium-sensitive potassium channel in the tonoplast of *Chara corallina*. *J. Membr. Biol.* 109: 9–19.

Bertl, A., C. L. Slayman, and D. Gradmann. 1993. Gating and conductance in an outward-rectifying K^+ channel from the plasma membrane of *Saccharomyces cerevisiae*. *J. Membr. Biol.* 132:183–199.

Blatz, A. L., and K. L. Magleby. 1986. Correcting single channel data for missed events. *Biophys. J.* 49:967–980.

Cecchi, X., D. Wolff, O. Alvarez, and R. Latorre. 1987. Mechanisms of Cs^+ blockade in a Ca^{2+}-activated K^+ channel from smooth muscle. *Biophys. J.* 52:707–716.

Colquhoun, D., and F. J. Sigworth. 1983. Fitting and statistical analysis of single channel records. *In* Single-Channel Recording. B. Sakmann and E. Neher, editors. Plenum Press, New York. 191–263.

Crouzy, S. C., and F. J. Sigworth. 1990. Yet another approach to the dwell-time omission problem of single-channel analysis. *Biophys. J.* 58: 731–743.

De Biasi, M., J. A. Drewe, G. E. Kirsch, and A. M. Brown. 1993. Histidine substitution identifies a surface position and confers CS^+ selectivity on a K^+ pore. *Biophys. J.* 65:1235–1242.

Demo, S. D., and G. Yellen. 1992. Ion effects on gating of the Ca^{2+}-activated K^+ channel correlate with occupancy of the pore. *Biophys. J.* 61:639–648.

Draber, S., R. Schultze, and U.-P. Hansen. 1991. Patch-clamp studies on the anomalous mole fraction effect of the K^+-channel in cytoplasmic droplets of *Nitella*: an attempt to distinguish between a multi-ion single-file pore and an enzyme kinetic model with lazy state. *J. Membr. Biol.* 123:183–190.

Draber, S., R. Schultze, and U.-P. Hansen. 1993. Cooperative behavior of K^+ channels in the tonoplast of *Chara corallina*. *Biophys. J.* 65: 1553–1559.

Draber, S., and R. Schultze. 1994. Correction for missed events based on a realistic model of a detector. *Biophys. J.* 66:191–201.

Durell, S. R., and H. R. Guy. 1992. Atomic scale structure and functional models of voltage-gated potassium channels. *Biophys. J.* 62:238–250.

Fisahn, J., U.-P. Hansen, and D. Gradmann. 1986. Determination of charge, stoichiometry and reaction constants from I/V-curve studies on a K^+ transporter in *Nitella*. *J. Membr. Biol.* 94:245–252.

FitzHugh, R. 1983. Statistical properties of the asymmetric random telegraph signal with application to single-channel analysis. *Math. Biosci.* 64:75–89.

Goldstein, S. A. N., and C. Miller. 1992. A point mutation in a *Shaker* K^+ channel changes its charybdotoxin binding site from low to high affinity. *Biophys. J.* 62:5–7.

Goldstein, S. A. N., and C. Miller. 1993. Mechanism of charybdotoxin block of a voltage-gated K^+ channel. *Biophys. J.* 65:1613–1619.

Gorman, A. L. F., J. C. Woolum, and M. C. Cornwall. 1982. Selectivity of the Ca^{2+}-activated and light-dependent K^+ channels for monovalent ions. *Biophys. J.* 38:319–322.

Gradmann, D., H. G. Klieber, and U.-P. Hansen. 1987. Reaction kinetic parameters for ion transport from steady state current-voltage curves. *Biophys. J.* 51:569–589.

Hagiwara, S., S. Miyazaki, and N. P. Rosenthal. 1976. Potassium current and the effect of caesium on this current during anomalous rectification of the egg cell membrane of a starfish. *J. Gen. Physiol.* 67: 621–638.

Hansen, U.-P., D. Gradmann, D. Sanders, and C. L. Slayman. 1981. Interpretation of current-voltage relationships for "active" ion transport systems. I. Steady-state reaction-kinetic analysis of class-I mechanisms. *J. Membr. Biol.* 63:165–190.

Hawkes, A. G., A. Jalali, and D. Colquhoun. 1990. The distribution of the apparent open times and shut times in a single channel record when brief events cannot be detected. *Phil. Trans. R. Soc. Lond. A.* 332:511–538.

Heinemann, S. H., and F. J. Sigworth. 1988. Open channel noise. IV. Estimation of rapid kinetics of formamide block in gramicidin A channels. *Biophys. J.* 54:757–764.

Hille, B., and W. Schwarz. 1978. Potassium channels as multi-ion single-file pores. *J. Gen. Physiol.* 72:409–442.

Hodgkin, A. L., and R. D. Keynes. 1955. The potassium permeability of a giant nerve fibre. *J. Physiol.* 128:61–88.

Jan, L. Y., and Y. N. Jan. 1992. Structural elements involved in specific K^+ channel functions. *Annu. Rev. Physiol.* 54:537–555.

Kirsch, G. E., J. A. Drewe, M. Taglialatela, R. H. Joho, M. DeBiasi, H. A. Hartmann, and A. M. Brown. 1992. A single nonpolar residue in the deep pore of related K^+ channels acts as a K^+:Rb^+ conductance switch. *Biophys. J.* 62:136–144.

Klieber, H.-G., and D. Gradmann. 1993. Enzyme kinetics of the prime K^+ channel in the tonoplast of *Chara*: selectivity and inhibition. *J. Membr. Biol.* 132:253–265.

Laver, D. R. 1992. Divalent cation block and monovalent cations in the large-conductance. K^+ channel from *Chara australis*. *J. Gen. Physiol.* 100:269–300.

Lühring, H. E. 1986. Recording of single K^+ channels in the membrane of cytoplasmic drop of *Chara australis*. *Protoplasma.* 133:19–28.

MacKinnon, R. 1991. Determination of the subunit stoichiometry of a voltage-activated potassium channel. *Nature (Lond.).* 350:232–235.

MacKinnon, R., and C. Miller. 1989. Mutant potassium channels with altered binding of charybdotoxin, a pore-blocking peptide inhibitor. *Science (Washington DC).* 245:1382–1385.

Magleby, A. L., and D. S. Weiss. 1990. Estimating kinetic parameters for single channels with simulation. A general method that resolves the missed event problem and accounts for noise. *Biophys. J.* 58:1411–1426.

Miller, C. 1991. 1990: Annus mirabilis of potassium channels. *Science (Washington DC).* 252:1092–1096.

Milne, R. K., G. F. Yeo, B. W. Madsen, and R. O. Edeson. 1989. Estimation of single channel kinetic parameters from data subject to limited time resolution. *Biophys. J.* 55:673–676.

Park, C.-S., and C. Miller. 1992. Mapping function to structure in a channel-blocking peptide: electrostatic mutants of charybdotoxin. *Biochemistry.* 31:7749–7755.

Roux, B., and R. Sauvé. 1985. A general solution to the time interval omission problem applied to single channel analysis. *Biophys. J.* 48:149–158.

Sakano, K., and M. Tazawa. 1986. Tonoplast origin of the envelope membrane of cytoplasmic droplets prepared from *Chara* internodal cells. *Protoplasma.* 131:247–249.

Schultze, R., and S. Draber. 1993. A nonlinear filter algorithm for the detection of jumps in patch-clamp data. *J. Membr. Biol.* 132:41–52.

Sigworth, F. J., and S. M. Sine. 1987. Data transformations for improved display and fitting of single-channel dwell time histograms. *Biophys. J.* 52:1047–1054.

Tanabe, T., H. Takeshima, A. Mikami, V. Flockerzi, H. Takahashi, K. Kangawa, M. Kojima, H. Matsuo, T. Hirose, and S. Numa. 1987. Primary structure of the receptor for calcium channel blockers from skeletal muscle. *Nature (Lond.).* 328:313–318.

Tester, M. 1988. Potassium channels in the plasmalemma of *Chara corallina* are multi-ion pores: voltage-dependent blockade by Cs^+ and anomalous permeabilities. *J. Membr. Biol.* 105:87–94.

Woodhull, A. M. 1973. Ionic blockage of sodium channels in nerve. *J. Gen. Physiol.* 61:687–708.

Yellen, G. 1984. Ionic permeation and blockade in Ca^{2+}-activated K^+ channels of bovine chromaffin cells. *J. Gen. Physiol.* 84:157–186.

Yeo, G. F., R. K. Milne, R. O. Edeson, and B. W. Madsen. 1988. Statistical interference from single channel records: two-state Markov model with limited time resolution. *Proc. R. Soc. Lond. B Biol. Sci.* 235:63–94.